Dalton Transactions

Accepted Manuscript

ROYAL SOCIETY OF CHEMISTRY

www.rsc.org/dalton

Ce^{3+} Sensitized $GdPO_4$:Tb^{3+} with Iron Oxide Nanoparticles: A Potential Biphasic System for Cancer Theranostics

Niroj Kumar Sahu, Naorem Shanta Singh, Lina Pradhan, Dhirendra Bahadur*

Department of Metallurgical Engineering and Materials Science, Indian Institute of Technology Bombay, Mumbai-400 076, India

*Corresponding author: dhirenb@iitb.ac.in, Tel: +91-22-25767632, Fax: +91-22-2576 3480

Abstract

We report a biphasic system (BPS) consisting of PEGylated Tb^{3+}-doped $GdPO_4$ nanorice sensitized with Ce^{3+} (PEG-NRs) and glutamic acid coated iron oxide nanoparticles (IONPs) with multifunctional capabilities. The mesoporous PEG-NRs exhibit green light luminescence property and high degree of aqueous stability. Its drug loading and release capacities were investigated for anti-cancer chemo doxorubicin (DOX). Its mesoporous nature and availability of plenty negatively charged functional group ($-COO^-$) on the surface of PEG-NRs facilitates approximately 94 wt. % DOX loading. In vitro studies carried out for PEG-NRs and its biphasic integrated system with iron oxide using HeLa and MCF-7 cell lines demonstrated its cell killing efficacy. The green luminescent observed under confocal laser scanning microscopy (CLSM) confirms the cellular uptake of PEG-NRs by HeLa cell lines and its accumulation in the cytoplasm. Approximately 50–55% of HeLa and MCF-7 cell death was observed after 24 h of incubation with DOX loaded BPS (2 mg IONPs and 0.25 mg PEG-NRs+DOX) which further increased to about 90 % when exposed to AC magnetic field (AMF) for 25 min. Our findings demonstrate that the therapeutic efficacy of BPS loaded with DOX could be a powerful multimodal system for imaging and synergistic chemo-thermal cancer therapy.

Keywords: PEGylation, $GdPO_4$ Nanorice, Iron oxide Nanoparticle, Biphasic system, Drug delivery, Cancer, Theranostics.

1. Introduction

Development of multifunctional nanoparticles has become one of the focus areas for various biological applications. Amongst these, fabrication and designing of highly efficient site specific drug delivery (DD) systems have gained importance recently.[1-5] During the last decade, there have been many reports on various types of DD systems including magnetic nanocomposite,[6] dendrimer,[7] polymeric and oxide nanoparticles,[8, 9] mesoporous silica nanoparticles (MSNs) etc.[10, 11] These DD systems combined with fluorescent molecules such as dyes, semiconductor quantum dots etc. have been utilized for real time monitoring during the drug transport.[12, 13] Recently, lanthanide based rare earth oxides have become promising as an alternative to conventionally used luminescent labels (dyes and semiconductor quantum dots).[14] This is due to their attractive optical properties, high chemical and photochemical stability and low toxicity along with their resistance to photobleaching, blinking, photochemical degradation and large Stokes shift.[11, 15-17]

Among various such oxides, $GdPO_4$ doped with lanthanide ions is an outstanding luminescent material for applications like display devices and biological imaging.[16, 18-20] The use of Gd^{3+} based nanophosphors as multifunctional platform for magnetic resonance (MR) and optical imaging has been lately reported.[16, 21] The possibility of combining optical imaging with a drug carrier will serve as an imaging probe to locate disease sites and as a carrier to precisely target the delivery of therapeutics, thus minimizing side effects on neighboring tissues or organs.[19, 22-27] Xu *et al*. recently reported urchin-like $GdPO_4:Eu^{3+}$ hollow spheres for simultaneous drug delivery of Ibuprofen and for bio imaging applications.[19] Also, Huang *et al*.[28] demonstrated the possibility of the use of self-assembled hydrogel like $GdPO_4 \cdot H_2O$ for drug delivery. In this context, functionalization of nanoparticles with free functional group(s) on the surface allows for the conjugation of different biomolecules, proteins, drugs etc.[29] Therefore, an efficient functionalization of Gd^{3+}

based luminescent nanoparticles such as $GdPO_4:Ln^{3+}$ (Ln^{3+} = lanthanide ions) will pave the way for the development of a single entity with multiple functionalities such as T_1 contrast agent in magnetic resonance imaging (MRI), optical imaging and simultaneous transport of drug. These nanoparticles can also be made an upconversion luminescent material with suitable combination of doping of lanthanide ions like Yb^{3+}/Er^{3+}, Yb^{3+}/ Tm^{3+} etc.[16, 30, 31] These may be excited by a continuous-wave of near-infrared (NIR) that exhibits an unique narrow photoluminescence with higher energy (visible region). This makes it suitable for *in vivo* applications.[31] Also, NIR has more penetration depth in the tissues and hence advantageous.

Iron oxide nanoparticles (IONPs), on the other hand, can be of extra benefit towards combination of thermo and chemotherapy for the treatment of cancer. Under AC magnetic field (ACMF), IONPs can be used for the generation of hyperthermia temperature causing death of the tumor cells. Also, ACMF is known to enhance the therapeutic efficacy of anticancer drug such as doxorubicin (DOX).[32-34]

In view of the attractive properties of the two systems, in the present work, we report a biphasic system (BPS) of these two constituents: (a) PEG-diacid coated $GdPO_4:Tb^{3+}/Ce^{3+}$ nanorice and (b) glutamic acid coated IONPs. The potential applications of this biphasic system were evaluated for chemotherapy and magnetic hyperthermia (Scheme 1). In addition, it is expected that such a system has the potential to be used for imaging and may be explored as T_1 and T_2 contrast agent in MRI.[35-37]

The individual components and their BPS are thoroughly characterized with X-ray diffraction (XRD), Fourier transform infrared (FTIR), dynamic light scattering (DLS) and electron microscopy. The fluorescence and thermal studies are employed to estimate the entrapment efficiency of drug in the carrier. The drug release in both the mild acidic (pH = 4.3) and physiological environments (pH = 7.4) is monitored with the fluorescence from

DOX. The cytotoxic effect of drug released from the DOX loaded PEG-NRs carrier (termed as PEG-NRs+DOX) has been investigated *in vitro* with HeLa (Human cervical carcinoma cells) and MCF-7 (breast cancer cell) cell lines. Further, the cytotoxicity effect due to chemo and thermal therapy of BPS loaded with DOX (termed as BPS+DOX) on Hela cells has been investigated towards the synergistic effect in killing the tumor cells.

2. Experimental section

2.1 Materials used

Analytical grade reagents were used as received. Gd_2O_3 (99.99%), $Tb(NO_3)_3{\cdot}6H_2O$ (99.99%), $Ce(NO_3)_3{\cdot}6H_2O$ (99.99%), $NH_4H_2PO_4$ (99.999%), $FeCl_3{\cdot}6H_2O$ (97%) and $FeCl_2{\cdot}4H_2O$ (99%) and Poly(ethylene glycol)bis(carboxy methyl)ether (HOOC-PEG-COOH, PEGD, M_w = 600) were purchased from Sigma-Aldrich Co. (St. Louis, MO, USA). Glutamic acid (GA), ethylene glycol (EG) and hydrochloric acid (HCl) were obtained from Merck India. MilliQ (18.2 MΩ-cm) water was used throughout the experiment. Dulbecco's modified eagle medium (DMEM), antibiotic-antimycotic solution (penicillin/streptomycin, P/S), Sulphorhodamine *B* (SRB), phosphate-buffered saline (PBS), Tris-buffered saline (TBS), trypsin-EDTA solution and trypan blue were obtained from Hi-Media Ltd (Mumbai, India). Acetic acid (glacial, 100%, Merck), paraformaldehyde (95%, Merck), trichloroacetic acid (TCA, 20% W/V, Loba Chemicals) and doxorubicin hydrochloride (DOX, ≥98%, Sigma Aldrich) were used in the experiment. L929, HeLa and MCF-7 cell lines were procured from the National Center of Cell Science (NCCS, Pune, India).

2.2 Synthesis of PEG-NRs, IONPs and BPS

The PEG-NRs were synthesized by a polyol method using EG as solvent following the earlier reports.[18] In a typical synthesis of the 5 at.% Ce^{3+} sensitized Tb^{3+} (5 at.%) doped $GdPO_4$ NRs, 350 mg of Gd_2O_3 and 49 mg of $Tb(NO_3)_3{\cdot}6H_2O$ along with 47 mg of $Ce(NO_3)_3{\cdot}6H_2O$ were dissolved in 1 mL concentrated HCl (35 vol.%) to convert the oxide

and nitrate precursors to their respective chloride counterparts. The excessive acid was removed by evaporating the solution through successive addition of milliQ water. This is repeated several times until the pH of the solution is nearly neutral. The above chloride solution was mixed with 30 mL of EG, 10 g of PEGD and 250 mg of $(NH_4)H_2PO_4$ in a reaction flask at 30 ºC. The solution was magnetically stirred for 30 min and the temperature was raised slowly to 150 °C and heated for 1 h resulting in the formation of white precipitate. The precipitates were washed thoroughly with methanol and collected by centrifugation.

The IONPs were prepared by co-precipitation method. In a typical synthesis procedure, 730 mg of $FeCl_3 \cdot 6H_2O$ and 270 mg of $FeCl_2 \cdot 4H_2O$ were dissolved in 50 mL of milliQ water in a round bottom flask and heated to 70 ºC with constant mechanical stirring (1000 rpm) under nitrogen atmosphere for 1 h. To this solution, 30 mL of ammonia hydroxide was added drop wise through a burette resulting in the formation of black precipitate. Then, 2 g of glutamic acid dissolved in 5 mL of water (previously prepared) was added to the reaction flask and heated at 90 ºC for another 1 h. Finally particles were washed with water and ethanol and collected by magnetic separation.

The BPS of PEG-NRs and IONPs has been prepared by taking 2 mg of IONPs and 0.25 mg of PEG-NRs. Both the materials were dispersed thoroughly in two separate glass vials containing 2 mL milliQ water. Then two dispersions were mixed in a single vial and put in a shaker for 48 h. Finally, the materials termed as BPS were collected by centrifugation. The IONPs, PEG-NRs and BPS are quite stable in the suspension as shown in the photographic images of their respective dispersed solutions (ESI Fig. S1).

2.3 Preparation of PEG-NRs+DOX and BPS+DOX

To prepare DOX loaded PEG-NRs, 10 mg of the PEG-NRs was thoroughly dispersed in 1 mL of water and later 50 µg of DOX solution (conc. 1 mg/mL) was added to the above solution. The whole solution was incubated in a dark environment with constant shaking for

24 h. The loaded part was separated from the supernatant through centrifugation. The fluorescence spectra of the supernatant were recorded to calculate the entrapment efficacy. For the preparation of BPS+DOX, same method was followed. The above prepared PEG-NRs+DOX *and* BPS+DOX were used for *in-vitro* study.

2.4 Drug release studies

Drug release from PEG-NRs+DOX was performed at physiological pH (7.4) and mild acidic pH (4.3) environments. DOX loaded PEG-NRs were dispersed in 1 ml of buffer solution and transferred inside two separate membranes (Himedia, Dialysis membrane-150, LA401) with phosphate-buffered saline (PBS) of pH = 7.4 and sodium acetate buffer of pH = 4.3, respectively. The membranes with the samples were kept in 20 mL PBS solution bath separately with constant stirring. The drug released from membranes into the PBS solution was collected at different time durations for analysis. The released DOX in the PBS was measured from fluorescence emission spectrum and percentage of release was estimated from fluorescence intensity. All the release experiments were performed in triplicate.

2.5 In vitro cell culture and cytotoxicity studies

The cell culture experiments were carried out using L929, HeLa and MCF-7 cell lines. The cells were harvested in DMEM supplemented with 10% PBS and 1% P/S solution at 37 ºC in a saturated humidified environment of 5% CO_2 atmosphere (InCu-safe). *In vitro* cytocompatibility of the NRs and BPS were evaluated by SRB assay using L929, Hela and MCF-7 cell lines.[38] In brief, the cells were seeded into 96-well plates (10,000 cells/well) and allowed to grow for 24 h. The cells adhered loosely on the surface were washed with PBS. The cells were then incubated with different concentrations of the samples. After 24 h the plates were thoroughly washed with PBS and air-dried to remove excess water before processing for SRB assay. For cell fixation, 100 µL of ice-cold 10% TCA was added into each well at 4 °C for 1 h which were further washed with deionized water and air-dried. 100

µL of 0.057% SRB was added and kept at room temperature for 20 min. Unbound SRB was washed away with 1% acetic acid (100 µL). To solubilize the dye, 100 µL of 10 mM TBS was added to each well and kept for 20 min. Thereafter, the plates were placed on a shaker to allow mixing and the absorbance (optical density, OD) was measured using a microplate spectrophotometer at 560 nm. The experiment was performed in triplicates. The percentage of viable cells was estimated using the formula:

$$\%\ \text{Cell viability} = \frac{\text{OD of treated cells}}{\text{OD of control cells}} \times 100$$

2.6 Cellular uptake of NPs

Approximately 10,000 HeLa cells were seeded on glass cover-slip placed in a 24-well culture plate and were allowed to grow overnight as a monolayer. The surface adhered cells were then incubated with fresh media containing 0.1 mg per mL of PEG-NRs and PEG-NRs+DOX for 24 h and later the cells were washed thoroughly with PBS and fixed with 300 µL of 10% paraformaldehyde. The excess paraformaldehyde was washed with PBS after 10 min. For confocal imaging the cover slips were placed on a glass slide and two-channel optical images of DOX and $GdPO_4:Ce^{3+}/Tb^{3+}$ were collected (470 and 435 nm excitation; 590 and 544 nm emission).

2.7 In Vitro Hyperthermia study

The potential synergistic effect of BPS loaded with DOX (BPS+DOX) on adherent HeLa cells was investigated in presence/absence of ACMF. The detail mechanism of heat generation with magnetic nanoparticles under ACMF is given in the ESI. The viability of treated cells was determined by the trypan blue method.[11] Approximately, one million cells were cultivated in 30 mm petridish with 1 mL of DMEM supplemented by 10% PBS and 1% P/S at 37 ºC under 5% CO_2 atmosphere. After 24 h, cells were thoroughly washed with PBS and incubated with 1 mL sample of BPS+DOX (concentration 2.25 mg mL^{-1} which contains

2 mg of IONPs and 0.25 mg PEG-NRs) and maintained at 37 ºC for 6 h along with negative and positive controls in triplicates. The cell petridishes were then exposed to ACMF (250 kHz, 460 Oe) for 25 min and thus treated cells were maintained inside incubator for 24 h. To count the number of dead cells with hemocytometer, the petridishes were washed with PBS and trypsinized to collect in a micro-centrifuge tube. The obtained cell pellets after centrifugation at 2000 rpm were suspended in 900 µL of PBS and 100 µL of 0.4% trypan blue was added to stain the dead cells. The percentage of viability was estimated by the formula:

$$\%\ \text{Viability} = \frac{\text{Live cells}}{\text{Total cells}} \times 100$$

2.8 Characterizations

The identification and purity of the phase was confirmed by XRD using PANalytical diffractometer (X'pert PRO) with CuK_α radiation (λ = 1.5405 Å) and a Ni filter. FTIR spectra were recorded using Nicolet Instruments (Magna550) by KBr pellet technique. The field emission scanning electron microscopy (FESEM) and transmission electron microscopy (TEM) images were recorded using JEOL JEM-7600F and JEM-2011F, respectively. Zeta potentials and hydrodynamic diameters (using dynamic light scattering) were measured in DelsaNano C, Beckman coulter Inc. The specific surface area, pore volume and pore size distribution of the PEG-NRs were measured by Micromeritics instrument (ASAP 2020). The specific surface area is measured using multipoint Brunauer–Emmet–Teller (BET) method whereas, pore size distribution and total pore volume were determined by the Brunauer Joyner–Hallenda (BJH) method. Prior to measurements, the samples were outgassed at 90 ºC with a heating rate of 10 ºC/min for 1 h and then the temperature was raised up to 140 ºC and maintained overnight. The magnetization versus field (M-H) and zero field cooled-field cooled (ZFC-FC) measurements were carried out using magnetic properties measurement

system (MPMS, Quantum Design). Hyperthermia studies were carried in Easy Heat 8310 (Ambrell, UK). Photoluminescence spectra were recorded at room temperature with a Hitachi F-4500 fluorescence spectrometer with a 150 W Xe lamp as the excitation source. For DOX loading and release experiment, the Varian Cary Eclipse Fluorimeter was used. Confocal laser scanning microscopy (CLSM) images were recorded in Olympus Inverted Confocal Microscope (Model IX-81). The live/dead cells counting were performed in hemocytometer.

3. Results and discussion

3.1 Structural and microstructure Studies

The indexed XRD patterns of as-synthesized PEG-NRs, IONPs and BPS are shown in Fig. 1. The PEG-NRs crystallizes in monoclinic phase of $GdPO_4$ (JCPDS#32–0386) whereas that of IONPs in inverse spinel Fe_3O_4 (JCPDS#19-0629). The estimated lattice parameter of IONPs is 8.378 Å and that of PEG-NRs are: a =6.67 Å, b = 6.86 Å and c = 6.31 Å and β = 104.14°. The estimated crystallite size of IONPs and PEG-NRs using Scherrer formula by considering most intense peak in XRD patterns are ~9.4 and 14.7 nm, respectively. The BPS exhibits the peaks of the above two phases. The surface chemical structure of the PEGylated NRs and glutamic acid coated IONPs were characterized by FTIR spectroscopy (Fig. 2). The characteristic bands of HOOC–PEG–COOH at 1092 cm^{-1} (C–O–C stretch) and 1412 cm^{-1} (CH_2 scissor) appear in the spectrum (Fig. 2a). A red shift in the above two bands are observed from that of the sole PEGD which may be attributed to the attachment of PEGD on the surface of $GdPO_4:Tb^{3+}/Ce^{3+}$. The carboxyl band at 1746 cm^{-1} in the spectrum of PEGD is shifted to 1626 cm^{-1} in NRs. This spectral change indicates the binding of carboxylate groups to the metal ions of $GdPO_4:Tb^{3+}/Ce^{3+}$ via the interaction of one or two oxygen atoms with the metal ions on the surface through covalent bond.[35, 39, 40] The presence of these organic functional groups on the surface of particles has also been confirmed from thermal studies (ESI, Fig. S2). The bands at 2880 and 2940 cm^{-1} correspond to the symmetric and

asymmetric stretching vibrations of the CH_2 group respectively. The O-H stretching vibration of carboxyl group is observed at 3458 cm^{-1}. The IR active bands of $(PO_4)^{3-}$ group (v_4) are observed at 540 and 637 while the v_3 is found to be merged with the C–O–C stretching band.

The FTIR spectra of GA coated IONPs along with the bare GA is presented in Fig. 2b. The bands at 1630 and 1421 cm^{-1} correspond to the carboxylate group and indicate the coating of glutamic acid on surface of IONPs.[40] The bands centered at 588 cm^{-1} is due to vibration of Fe-O of Fe_3O_4 and 618 cm^{-1} is probably assigned to the existence of maghemite (γ-Fe_2O_3) phase due to surface oxidation.[41] Additionally, the enhanced peaks at 2935 and 2844 cm^{-1} observed are due to the symmetric and asymmetric CH_2 stretching vibrations respectively.[42] A broad band centered at 3415 cm^{-1} is assigned to the merge of the asymmetric stretching modes of NH_2 group and O-H stretching vibration of the carboxyl group present in the glutamic acid.[43]

The nitrogen (N_2) adsorption–desorption isotherm indicates the mesoporous nature of PEG-NRs (Fig. 3a). It possesses a specific surface area of 88 m^2 g^{-1} and pore size distribution of average pore diameter ~16 nm. The porous nature of PEG-NRs assemblies is derived from swelling of polymeric PEG corona which is confirmed by the disappearance of pores in the sample when heated at 450 °C for 2 h (Fig. 3b). The mesoporous nature and large specific surface area of PEG-NRs make it an ideal nanocarrier for drug delivery applications.

Fig. 4a,b display the FESEM and TEM images of the PEG-NRs. The images show the presence of the nanorice shaped $GdPO_4$:Tb^{3+}/Ce^{3+} nanoparticles. The NRs are of uniform size with average diameter and length of 10 and 60 nm, respectively. The selected area electron diffraction (SAED) pattern shows that the samples are crystalline in nature. The indexed planes from SAED and the calculated *d*-spacing of 0.30 nm measured from HRTEM image matched with the (120) plane of monoclinic $GdPO_4$ and are shown in supplementary information (ESI, Fig. S3a,b). Fig. 4c shows the TEM image of IONPs indicating the

presence of dispersed nanoparticles with a size of ~12 nm. The SAED pattern is well indexed with the inverse spinel structure and characteristic *d*-spacing of 0.30 nm which is related to the (220) plane (ESI Fig. S3c,d). Fig. 4d shows the TEM image of the BPS of PEG-NRs and IONPs. We do not see a clear evidence of attachment of IONPs on PEG-NRs in TEM. In fact, it more looks like a biphasic system of the two phases. However, some of the other results such as hydrodynamic diameter, change in zeta potential and EDX mapping suggest that some amount of iron oxide might be conjugated/adsorbed on PEG-NRs surface discussed later in the text. The EDX mapping shows the uniform distribution of Gd, Ce, Tb and Fe throughout the sample area scanned (ESI Fig. S4). As glutamic acid (2-aminopentanedioic acid) is coated on IONP, the $-NH_3^+$ group available on the surface might have helped for such uniformity as it may get attached to the negative carboxyl group on the surface of NRs. However, the extent of attachment may not be significant as the surface of IONPS also contains abundant of negatively charged functional group ($-COO^-$). If both the species will be oppositely charged they may get attached through ionic interaction but the colloidal stability is a measure concern due to charge neutrality which is not happen in BPS and hence more advantageous (ESI Fig. S1).

3.2 Magnetic properties

Fig. 5 shows the plot of magnetization versus applied field (M-H) for PEG-NRs, IONPs and BPS. The PEG-NRs shows paramagnetic behavior due to half-filled $4f^7$ outermost orbital of Gd^{3+}. IONPs show a typical superparamagnetic behavior with a magnetization of 62 emu/g measured at 20 KOe. The superparamagnetic nature is further confirmed by ZFC-FC measurement (applied field = 100 Oe) with a blocking temperature at 150 K (inset of Fig. 5). The BPS shows a similar behavior with lower magnetization value (30 emu/g). The highly paramagnetic nature of PEG-NRs and the superparamagnetic nature of IONPs can be efficiently utilized for longitudinal (T_1-weighted) and transverse (T_2-weighted) relaxation

contrast agents in MRI respectively.[44] Also, the advantage of this system is that even if they are not forming core-shell or composite type structure, still they can be localized to the specific target site with the application of magnetic field as both are highly magnetic (paramagnetic/superparamagnetic) in nature.

3.3 Photoluminescence study

Excitation spectrum of PEG-NRs with a monitoring emission at 544 nm (green) is shown in supplementary information (Fig. S5). Absorption peaks are observed at 245, 280 and 315 nm. The first and second peaks are associated with the spin allowed 4*f*-5*d* transitions in Ce^{3+} from $^2F_{5/2}$ ground state of 4*f* to two different excited state levels of 5*d* whereas the third one is related to 4*f*-4*f* transition of Ce^{3+}. The excitation peaks observed at $^7F_6 \rightarrow {}^5G_5$ (355 nm), $^7F_6 \rightarrow {}^5L_{10}$ (373 nm) and $^7F_6 \rightarrow {}^5G_6$ (380 nm) are related to the *f-f* transition absorptions of Tb^{3+}. The peak of Gd^{3+} ion at ~ 278 nm which is due to $^8S_{7/2} \rightarrow {}^6I_{11/2}$ transition is not observed as it is merged with the spin allowed Ce^{3+} 4*f*-5*d* transitions. The presence of strong absorption peak (~280 nm) compared to 4*f*-4*f* transitions which are of spin forbidden nature indicates the occurrence of strong energy transfer from Ce^{3+}/Gd^{3+} to the excited energy states of Tb^{3+}. Fig. 6 shows the emission spectra of PEG-NRs and BPS after excitation at 280 nm. An enhanced emission from PEG-NRs is observed with strongest peak at 544 nm (green) due to sensitization with Ce^{3+}.[45] The emission bands at 490, 544, 585 and 620 nm in the spectrum are related to $^5D_4 \rightarrow {}^7F_6$, $^5D_4 \rightarrow {}^7F_5$, $^5D_4 \rightarrow {}^7F_4$ and $^5D_4 \rightarrow {}^7F_3$ transitions, respectively. Among these, 544 nm is strongest one giving intense green emission. Similarly, the spectrum of BPS also shows the characteristic emission peaks of Tb^{3+}. However, the intensity of luminescence is reduced due to the presence of IONPs since the magnetic particles quench the luminescence to a certain extent.[7]

3.4 Drug loading and release properties

Due to biocompatible nature of PEG-NRs and BPS with three different sets of cell lines viz. L929, MCF-7 and HeLa (more than 80% cell viability in the cases studied as illustrated in ESI, Fig. S6), these functionalized particles can be promising candidates for use as drug delivery host to carry a high payload of drug molecules. The entrapment efficiency of drug in PEG-NRs has been monitored with fluorescence intensity of DOX (supernatant) separated from loaded sample. A very high entrapment efficiency of ~94% is primarily due to porous nature and significant specific surface area of PEG-NRs. In addition they possess a large number of free carboxyl groups ($-COO^-$) on the surface which can bind electrostatically with amine groups of DOX. The polymeric nature of PEG-diacid also plays an additional role for higher entrapment. This can be realized from TGA data (Fig. S2). The number of PEG molecules grafted on 10 mg of the PEG-NRs is estimated as $\sim 1.3\times10^{18}$ which is more than $\sim 5.5\times10^{16}$ of DOX molecules present in 50 µg loaded. There is an additional loss of weight (~2.5%) above ~420 °C in PEG-NRs+DOX compared to PEG-NRs. The high payload of drug molecules in different carriers has also been reported earlier.[5, 46] It has also been observed that when $GdPO_4$ nanoparticles are coated with PEG-3000 (ESI Fig. S7) instead of PEG-diacid, the loading efficiency achieved is ~30 wt.% only. This has been clearly indicated in the decrease profile of fluorescence intensity of DOX (unloaded part) after loading with the above materials (ESI Fig. S8). It may be mentioned that the attachment of DOX on to the surface of IONPs is very small as is evident from the fluorescence spectra (ESI Fig. S8).

Fig. 7 shows the DOX release profiles from bare DOX (control) during 6 h and PEG-NRs+DOX over a period of 150 h at physiological pH = 7.4 and mild acidic pH = 4.3 which mimics the endosomal environment of cancer cells. The overall release of DOX from PEG-NRs+DOX in both environments show essentially sustained release pattern. The drug release

profiles have two distinct linear rates. The initial stage of burst release up to 14 h (inset of Fig. 7), during which 16.4 ± 2.4 % and 46.1 ± 1.4 % of DOX were released from the sample at pH 7.4 and 4.3, respectively can be attributed to the release of surface adsorbed drug molecules.[9] Moreover, the faster diffusion rate at initial stage may be due to the higher concentration gradient of drug from matrix to the release medium which slows down steadily with passage of time as the equilibrium is attained. The release beyond 14 h is much slower. It is worthwhile to mention that similar results are reported in several publications.[4, 9, 47, 48] We believe that the role of concentration gradient is very important and such an explanation is given in literature.[9] To understand this kind of behavior, a detailed study is required considering the viscosity and concentration of ions in the reservoir and the sink in the drug release experiment. Also, pH plays an important role in the release; as the DOX is attached ionically with the surface carboxyl group of PEG-NRs. These bonds get cleaved faster in lower pH condition. This is in accordance with Higuchi drug release model confirming that the DOX release process is diffusion-controlled.[48] However, bare DOX is released in a rapid manner in both the conditions with marginally faster rate if the pH = 4.3. This supports our statement of drug entrapment/attachment on the particle surface in the previous paragraph. It is further observed that pH does not have any impact on fluorescence intensity of DOX as given in Fig. S9 (supplementary information). Hence, it is indicated that the mechanism of drug loading and release is dependent on the change in the nature of the chemical bonding of the drug molecule with the functionalized nanoparticles in different pH environments.

Interestingly, the overall release efficiency of the drug from PEG-NRs+DOX is higher at pH = 4.3 than at pH = 7.4 which is important for the killing of relatively acidic tumor cells. At pH = 4.3, nearly 45% of DOX is released during first 20 h and afterwards there is a gradual release with an overall cumulative release efficiency of 64% over a period of 170 h. On the other hand, the rate of release is much slower in physiological environment (pH = 7.4)

with ~15% release during first 20 h. The cumulative drug release efficiency over a period of 170 h is found to be 21%. This is because of the fact that in the acidic conditions, $-COO^-$ has the higher affinity towards abundant H^+ than $-NH_3^+$ thereby partially neutralizing the $-COO^-$ group and eventually weakening the electrostatic interaction between the DOX and $-COO^-$ on the surface of PEG-NRs. Moreover, the pKa value of carboxylate group is about ~4.8. So, carboxylate group may be dissociated in the solution (~ pH = 4.3) which helps in the weakening of bond between DOX and PEG-NRs. Also, if pH is decreased, increase protonation of $–NH_2$ groups on DOX may lead to enhanced drug release. Thus, the release is favored in acidic pH condition. These overall comparative results reveal the pH sensitivity of drug release and such observations have been reported in many different systems.[8, 11, 49]

3.5 In-vitro cytotoxicity study for PEG-NRs+DOX in HeLa and MCF-7 cells

The cytotoxicity effect of DOX released from PEG-NRs+DOX on two different human cancerous cell lines (HeLa and MCF-7) due to DOX release from PEG-NRs+DOX was investigated. The cytotoxicity due to different concentrations of PEG-NRs+DOX along with PEG-NRs as control is demonstrated in Fig. 8. The bare PEG-NRs show hardly any adverse effect against both the cell lines after 24 h of treatment (Fig. S6). However, a clear cytotoxic effect could be observed in the case of PEG-NRs+DOX due to the release of DOX in the cells. For both the cell lines, cytotoxic effect sequentially increases with the increase in concentration with maximum effect of ~70% (HeLa) and 68% (MCF-7) at 0.5 mg/mL of PEG-NRs+DOX (DOX content ~2.4 µg). The enhanced cytotoxicity with the increase in concentration thus resulted eventually more release of DOX inside the cells inducing cell death.

It is important to evaluate whether the carrier is internalized inside the cell or not. Fig. 9 shows the CLSM images of HeLa cells after incubating with PEG-NRs+DOX for 4 h.

While Fig. 9a shows the bright field image, the green and red fluorescence is obtained from the PEG-NRs (Fig. 9b) and DOX (Fig. 9c), respectively. The merged image (Fig. 9d) confirms the internalization of both carrier and DOX inside the cell through endocytosis and DOX accumulation inside the nucleus. A close observation shows that the presence of DOX (red fluorescence) is comparatively more in cytoplasm than inside the nuclei. This suggests that the DOX is released via cytoplasm to the nucleus suggesting the sustained release of DOX from the carrier.

3.6 Synergistic effect of PEG-NRs-IONPs+DOX

BPS which contains 2 mg of IONPs along with 0.25 mg PEG-NRs was loaded with DOX (DOX content ~1.2 μg). It is envisaged that such a biphasic system would be useful as a multimodal platform providing probe for imaging as well as advantageous for a combination therapy. While the porous PEG-NRs with its abundant negatively charged carboxyl ions on its surface is capable to load DOX, the GA coated IONPs by virtue of the negatively charged carboxyl groups may also attach to the positively charged $–NH_3^+$ groups of DOX to a certain extent. As it is indicated from the fluorescence spectra (Fig. S8), the loading of DOX on IONPs is very small, while most DOX is loaded on porous PEG-NRs. As discussed earlier in the text, the IONPs (2 mg) present in the system is able to generate the hyperthermia temperature (≥42 °C) under an applied ACMF (250 kHz, 460 Oe) which is due to Néel and Brownian relaxation losses (ESI, Fig. S10). On the other hand, most of the drug release occurs from PEG-NRs. Such a biphasic suspension (BPS) is very useful for a combination therapy.[50,51] Thus, the synergistic effect of chemotherapy and magnetic hyperthermia was further evaluated for HeLa and MCF-7 cell lines with BPS.

The viability (%) of HeLa and MCF-7 cells incubated with DOX in different formulation and conditions show the cell viability of ~ 48 ±3.5 and 49 ±4.7 %, respectively with chemotherapy alone using 0.25 mg of PEG-NRs+DOX (DOX content ~1.2 μg) (Fig.

10). Similarly, nearly the same level of toxicity to the cells is seen even with BPS+DOX in the absence of ACMF. However, the viability of ~10 ±3.7% (in HeLa) and 15 ±3.1% (in MCF-7) (~ 90% killing) is observed under the application of ACMF (250 kHz, 460 Oe) during 10 min exposure at 42 °C (took extra 16 min to reach 42 °C initially). It may be pointed out that with the DOX alone, ~20% (~80% killing) viability is observed. It may not be of much significance as the DOX is released instantly if it is bare (see Fig. 7). Thus, the presence of IONPs along with DOX has contributed to more cell death under the applied ACMF. This is because of the fact that cancer cells are more vulnerable and sensitive to the heat than normal cells as confirmed from the comparative cell viability of L292 and HeLa cells with or without the exposure of hyperthermia temperature (ESI, Fig. S11, S12). Also, the applied ACMF helps diffusion of drugs through bond breaking by the strong mechanical force generated by the magnetic particles under AC field thereby enhancing the drug release. Thus the enhanced effect towards the cancer therapy due to the synergistic effect of thermal and chemotherapy is evident. Fig. 11 shows the optical microscopic images of the HeLa cells in control and after treatment with and without the application of ACMF. The density of live cells is observed to decrease considerably compared to control (Fig. 11a) with the treatment of chemotherapy only with bare DOX (Fig. 11b) and BPS+DOX (Fig. 11c). A significant change in morphology is clearly seen. However, the density is substantially reduced when the same treatment was performed under the application of ACMF (Fig. 11d) due to the synergistic effect of both chemo and thermal therapy.

4. Conclusion

Multifunctional PEGylated Ce^{3+} sensitized and Tb^{3+} activated $GdPO_4$ nanorice has been synthesized using polyol method and used as a potential carrier of anticancer therapeutic. The biphasic system of PEG-NRs and IONPs has been formulated and investigated for simultaneous chemo-thermal therapy of HeLa and MCF-7 cells. The PEG-

NRs and BPS show the potential for carrying the DOX with high entrapment efficiency. CLSM images confirm the substantial internalization of drug loaded carrier into the cell. The drug release from PEG-NRs+DOX is pH sensitive and a better efficiency in tumor condition is seen. The cell death is ~50-55% in both HeLa and MCF-7 cells when treated with 0.25 mg of PEG-NRs+DOX which increases to more than 90% with BPS+DOX in hyperthermic condition. The synergistic effect of combined chemo and thermal therapy is evident. Hence, this system could efficiently be utilized as a multifunctional platform for pH stimulated drug delivery, bioimaging and chemothermal therapy for the treatment of cancer. In addition, it is expected that it may exhibit the potential to be used as MRI contrast agent.

Supplementary materials:

† Electronic supplementary information (ESI) available: TGA, TEM, EDX, Photoluminescence spectra, cell biocompatibility study, zeta potential and hydrodynamic diameter, hyperthermia etc. are described.

Acknowledgement

Authors are thankful to Nanomission of Department of Science and Technology (DST) and nanotechnology division of Department of Information Technology (DIT), Government of India for financial support. Fruitful discussion with Mr. Sunil Kumar, Department of Chemical Engineering, IIT Bombay is acknowledged. We also acknowledge the central characterization facilities at IIT Bombay.

References

[1] R. A. Petros and J. M. DeSimone, *Nat. Rev. Drug. Discov.* 2010, **9**, 615.

[2] S. R MacEwan, D. J. Callahan and A. Chilkoti, *Nanomedicine* 2010, **5**, 793.

[3] X. Guoand and F. C. Szoka Jr., *Acc. Chem. Res.* 2003, **36**, 335.

[4] L. Pradhan, R. Srivastava and D. Bahadur, *Acta Biomater* 2014, doi: 10.1016/j.actbio.2014.04.011.

[5] S. Kumar, A. Daverey, N. K. Sahu and D. Bahadur, *J. Mater. Chem. B* 2013, **1**, 3652.

[6] L. Zhu, D. Wang, X. Wei, X. Zhu, J. Li, C. Tu, Y. Su, J. Wu, B. Zhu and D. Yan, *J. Control. Release* 2013, **169**, 228.

[7] M. N. Luwang, S. Chandra, D. Bahadur and K. Srivastava, *J. Mater. Chem.* 2012, **22**, 3395.

[8] M. K. Jaiswal, M. Gogoi, H. Dev Sarma, R. Banerjee and D. Bahadur, *Biomater. Sci.*, 2014, **2**, 370.

[9] Y. Mi, X. Liu, J. Zhao, J. Ding and S. S. Feng, *Biomaterials* 2012, **33**, 7519.

[10] B. G. Trewyn, I. I. Slowing, S. Giri, H.-T. Chen and V. S. Y. Lin, *Accounts. Chem. Res.* 2007, **40**, 846.

[11] N. Shanta Singh, H. Kulkarni, L. Pradhan and D. Bahadur, *Nanotechnology* 2013, **24**, 065101.

[12] F. Wang, X. Chen, Z. Zhao, S. Tang, X. Huang, C. Lin, C. Cai and N. Zheng, *J. Mater. Chem.* 2011, **21**, 11244.

[13] F. Pinaud, X. Michalet, L. A. Bentolila, J. M. Tsay, S. Doose, J. J. Li, G. Iyer and S. Weiss, *Biomaterials* 2006, **27**, 1679.

[14] S. Gai, C. Li, P. Yang, J. Lin, *Chem. Rev.* 2014, **114**, 2343−2389.

[15] N. S. Singh, N. K. Sahu and D. Bahadur, *J. Mater. Chem. C* 2014, **2**, 548.

[16] W. L. Ren, G. Tian, L. J. Zhou, W. Y. Yin, L. Yan, S. Jin, Y. Zu, S. J. Li, Z. J. Gu and Y. L. Zhao, *Nanoscale* 2012, **4**, 3754.

[17] Y. L. Dai, P. A. Ma, Z. Y. Cheng, X. J. Kang, X. Zhang, Z. Y. Hou, C. X. Li, D. M. Yang, X. F. Zhai and J. Lin, *Acs Nano* 2012, **6**, 3327.

[18] N. K. Sahu, R. S. Ningthoujam and D. Bahadur, *J. Appl. Phys.* 2012, **112**, 014306.

[19] Z. H. Xu, Y. Cao, C. X. Li, P. A. Ma, X. F. Zhai, S. S. Huang, X. J. Kang, M. M. Shang, D. M. Yang, Y. L. Dai and J. Lin, *J. Mater. Chem.* 2011, **21**, 3686.

[20] S. Rodriguez-Liviano, A. I. Becerro, D. Alcantara, V. Grazu, J. M. de la Fuente and M. Ocana, *Inorg. Chem.* 2013, **52**, 647.

[21] M. J. Bailey, R. van der Weegen, P. J. Klemm, S. L. Baker and B. A. Helms, *Adv. Healthcare Mater.* 2012, **1**, 437.

[22] C. Wang, L. A. Cheng and Z. A. Liu, *Biomaterials* 2011, **32**, 1110.

[23] J. Shen, L. Zhao and G. Han, *Adv. Drug. Deliver. Rev.* 2013, **65**, 744.

[24] S. L. Gai, P. P. Yang, C. X. Li, W. X. Wang, Y. L. Dai, N. Niu and J. Lin, *Adv. Funct. Mater.* 2010, **20**, 1166.

[25] J. Kim, J. E. Lee, J. Lee, J. H. Yu, B. C. Kim, K. An, Y. Hwang, C. H. Shin, J. G. Park, J. Kim and T. Hyeon, *J. Am. Chem. Soc.* 2006, **128**, 688.

[26] M. Liong, J. Lu, M. Kovochich, T. Xia, S. G. Ruehm, A. E. Nel, F. Tamanoi, J. I. Zink, *Acs Nano* 2008, **2**, 889.

[27] F. Zhang, G. B. Braun, A. Pallaoro, Y. C. Zhang, Y. F. Shi, D. X. Cui, M. Moskovits, D. Y. Zhao and G. D. Stucky, *Nano Lett.* 2012, **12**, 61.

[28] C. C. Huang, Y. W. Lo, W. S. Kuo, J. R. Hwu, W. C. Su, D. B. Shieh and C. S. Yeh, *Langmuir* 2008, **24**, 8309.

[29] S. Mornet, S. Vasseur, F. Grasset and E. Duguet, *J. Mater. Chem.* 2004, **14**, 2161.

[30] X. J. Xie, N. Y. Gao, R. R. Deng, Q. Sun, Q. H. Xu and X. G. Liu, *J. Am. Chem. Soc.* 2013, **135**, 12608.

[31] Y. Dai, X. Kang, D. Yang, X. Li, X. Zhang, C. Li, Z. Hou, Z. Cheng, P. A. Ma, J. Lin, *Adv. Healthcare Mater.* 2013, **2**, 514.

[32] S. Brule, M. Levy, C. Wilhelm, D. Letourneur, F. Gazeau, C. Menager and C. Le Visage, *Adv. Mater.* 2011, **23**, 787.

[33] C. R. Thomas, D. P. Ferris, J. H. Lee, E. Choi, M. H. Cho, E. S. Kim, J. F. Stoddart, J. S. Shin, J. Cheon and J. I. Zink, *J. Am. Chem. Soc.* 2010, **132**, 10623.

[34] Y. Xu, A. Karmakar, W. E. Heberlein, T. Mustafa, A. R. Biris and A. S. Biris, *Adv. Healthcare Mater.* 2012, **1**, 493.

[35] F. Q. Hu, K. W. MacRenaris, E. A. Waters, E. A. Schultz-Sikma, A. L. Eckermann and T. J. Meade, *Chem. Commun.* 2010, **46**, 73.

[36] W.-Y. Huang and J. J. Davis, *Dalton Trans.* 2011, **40**, 6087

[37] A. K. Parchur, A. A. Ansari, B. P. Singh, T. N. Hasan, N. A. Syed, S. B. Raia and R. S. Ningthoujam, *Integr. Biol.*, 2014, **6**, 53.

[38] M. K. Jaiswal, R. Banerjee, P. Pradhan and D. Bahadur, *Colloid. Surface B*, 2010, **81**, 185.

[39] Q. X. Liu and Z. H. Xu, *Langmuir* 1995, **11**, 4617.

[40] B. Luo, S. A. Xu, A. Luo, W. R. Wang, S. L. Wang, J. Guo, Y. Lin, D. Y. Zhao and C. C. Wang, *Acs Nano*, 2011, **5**, 1428.

[41] X. H. Sun, C. M. Zheng, F. X. Zhang, Y. L. Yang, G. J. Wu, A. M. Yu and N. J. Guan, *J. Phys. Chem. C*, 2009, **113**, 16002.

[42] N. K. Sahu and D. Bahadur, *J. Appl. Phys.* **2013**, *113*, 134303.

[43] N. K. Sahu, A. Prakash and D. Bahadur, *Dalton Trans.*, 2014, **43**, 4892.

[44] H. B. Na, I. C. Song, T. Hyeon, *Adv. Mater.* 2009, **21**, 2133.

[45] N. K. Sahu, N. S. Singh, R. S. Ningthoujam and D. Bahadur, *ACS Photonics* 2014, **1**, 337.

[46] Y. H. Jia, M. Yuan, H. D. Yuan, X. L. Huang, X. Sui, X. M. Cui, F. Q. Tang, J. Peng, J. Y. Chen, S. B. Lu, W. J. Xu, L. Zhang and Q. Y. Guo, *Int. J. Nanomed.* 2012, **7**, 1697.

[47] W. Chen, F. Meng, R. Cheng and Z. Zhong, *J. Control. Release* 2010, **142**, 40.

[48] K. C. Barick, S. Singh, N. V. Jadhav, D. Bahadur, B. N. Pandey and P. A. Hassan, *Adv. Funct. Mater.* 2012, **22**, 4975.

[49] L. M. Pan, Q. J. He, J. N. Liu, Y. Chen, M. Ma, L. L. Zhang and J. L. Shi, *J. Am. Chem. Soc.* 2012, **134**, 5722.

[50] S. Chandra, S. Dietrich, H. Lang and D. Bahadur, *J. Mater. Chem.* 2011, **21**, 5729.

[51] M. Gogoi, H. D Sarma, D. Bahadur, R. Banerjee, *Nanomedicine* 2013, doi: 10.2217/nnm.13.90.

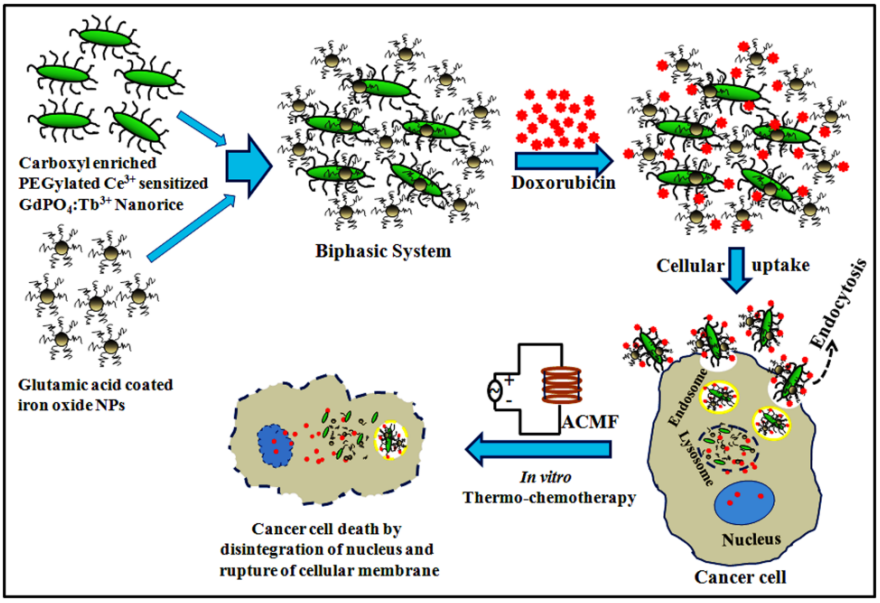

Scheme 1. Schematic representation of carboxyl enriched PEGylated Ce^{3+} sensitized $GdPO_4:Tb^{3+}$ nanorice (PEG-NRs) and its biphasic system (BPS) with glutamic acid coated iron oxide nanoparticles (IONPs) for the evaluation of their efficiency for chemo-thermal treatment against cancer cells.

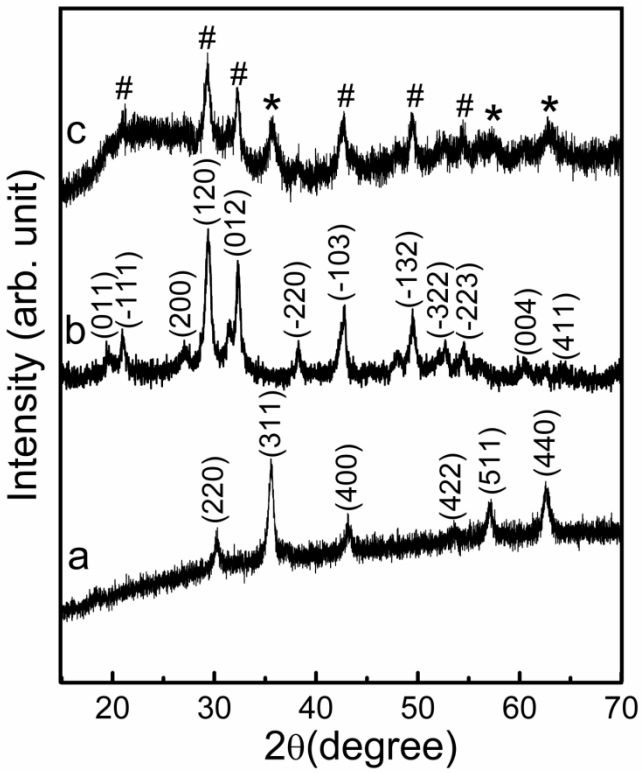

Fig. 1 XRD patterns of as-synthesized (a) IONPs, (b) PEG-NRs and (c) BPS. Symbol (*) and (#) in (c) represents Fe_3O_4 and $GdPO_4$:Tb^{3+}/Ce^{3+} phases, respectively.

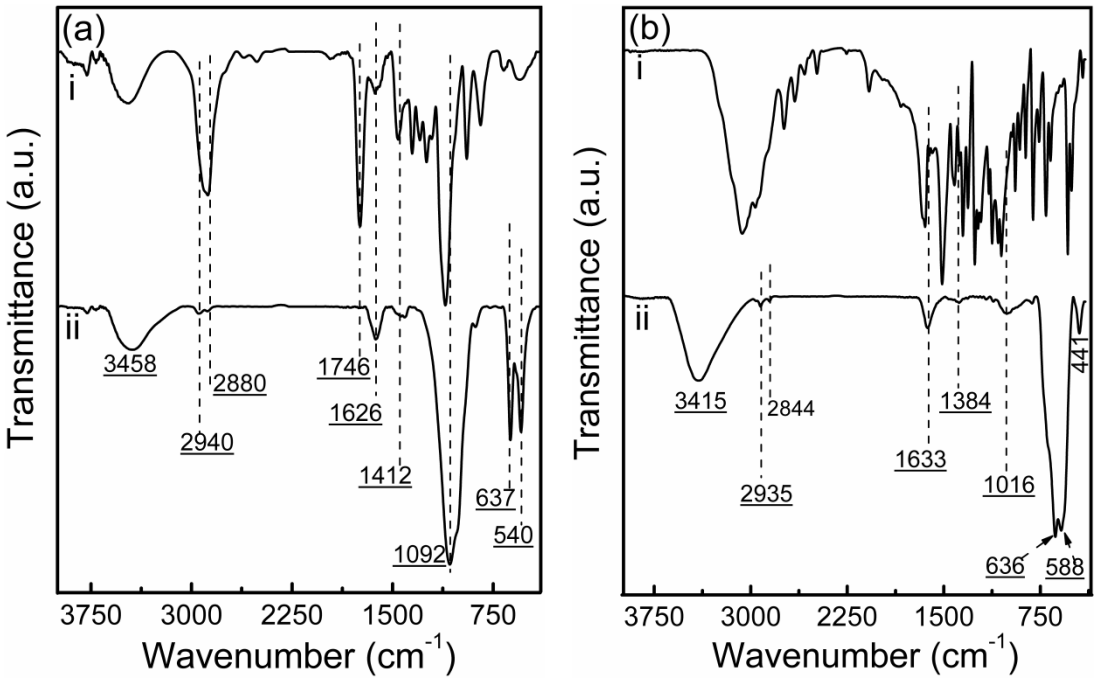

Fig. 2 FTIR spectra of (a-i) PEGD, (a-ii) PEG-NRs, (b-i) glutamic acid and (b-ii) IONPs.

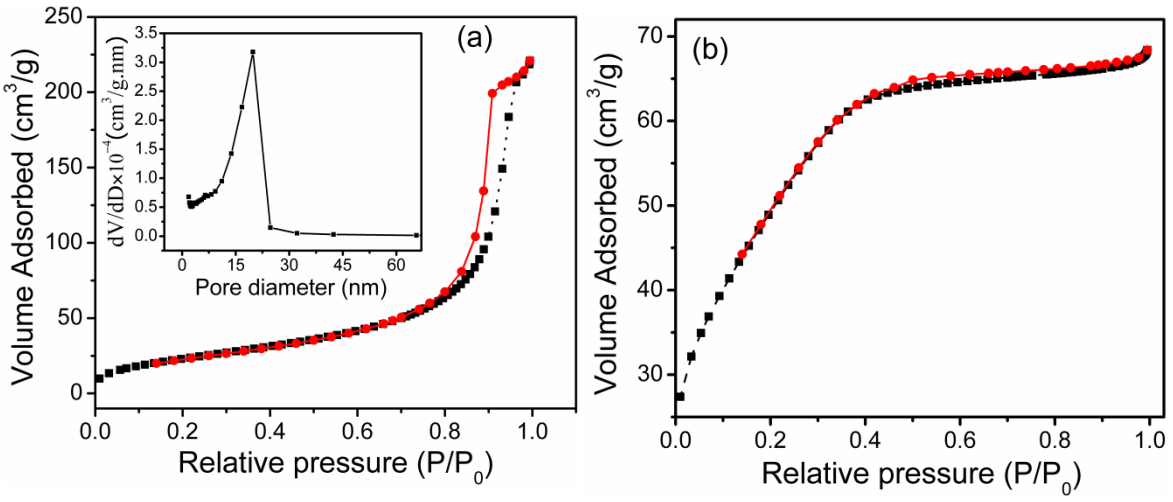

Fig. 3 Nitrogen adsorption/desorption isotherm of (a) as-synthesized and (b) 450 °C heated PEG-NRs. Inset of (a) shows the pore size distribution. The square (▪) and circle (•) symbols indicate adsorption and desorption branches.

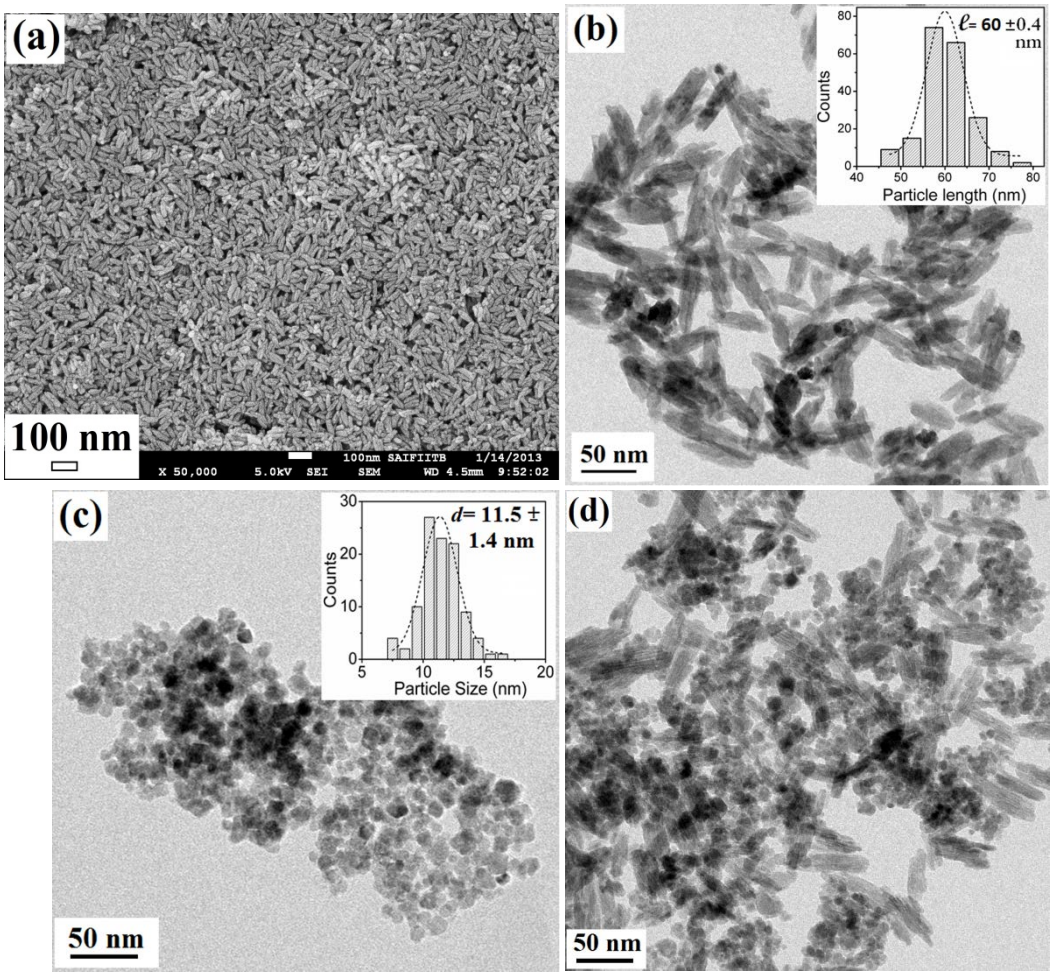

Fig. 4 (a) FESEM of the PEG-NRs. TEM images of (b) PEG-NRs, (c) IONPs and (d) BPS. Respective particle size distributions are shown in the insets of figure (b) and (c).

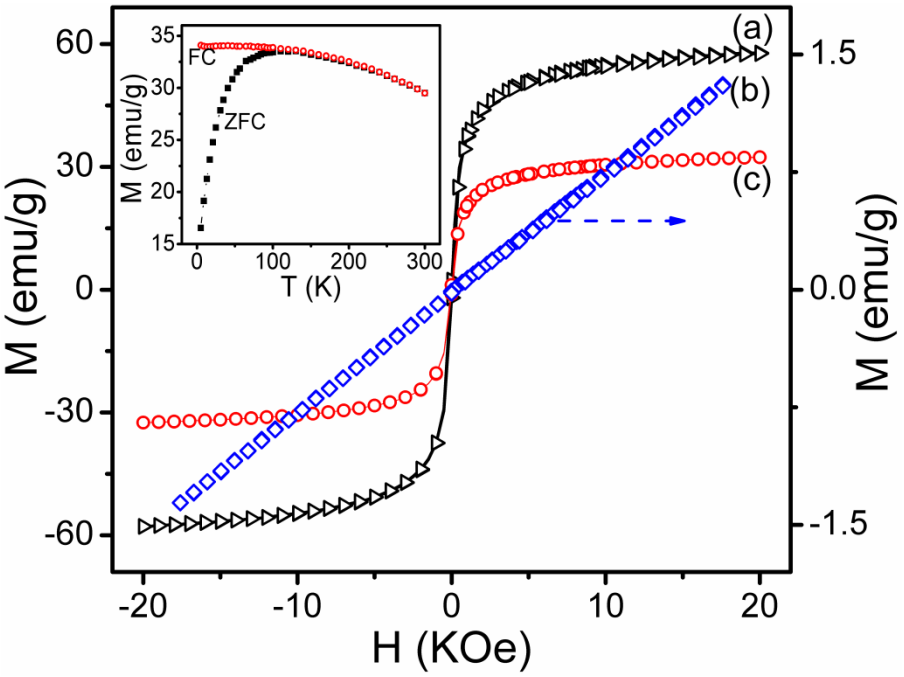

Fig. 5 M versus H plots of (a) IONPs, (b) PEG-NRs and (c) BPS. ZFC-FC plot of IONPs is shown in the inset.

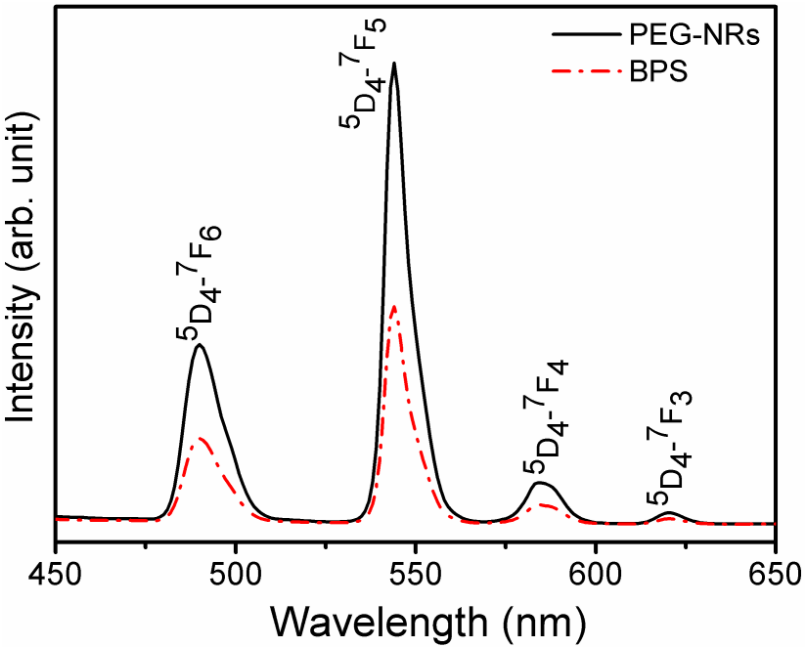

Fig. 6 Emission spectra of PEG-NRs and BPS after UV excitation (λ_{ex} = 280 nm).

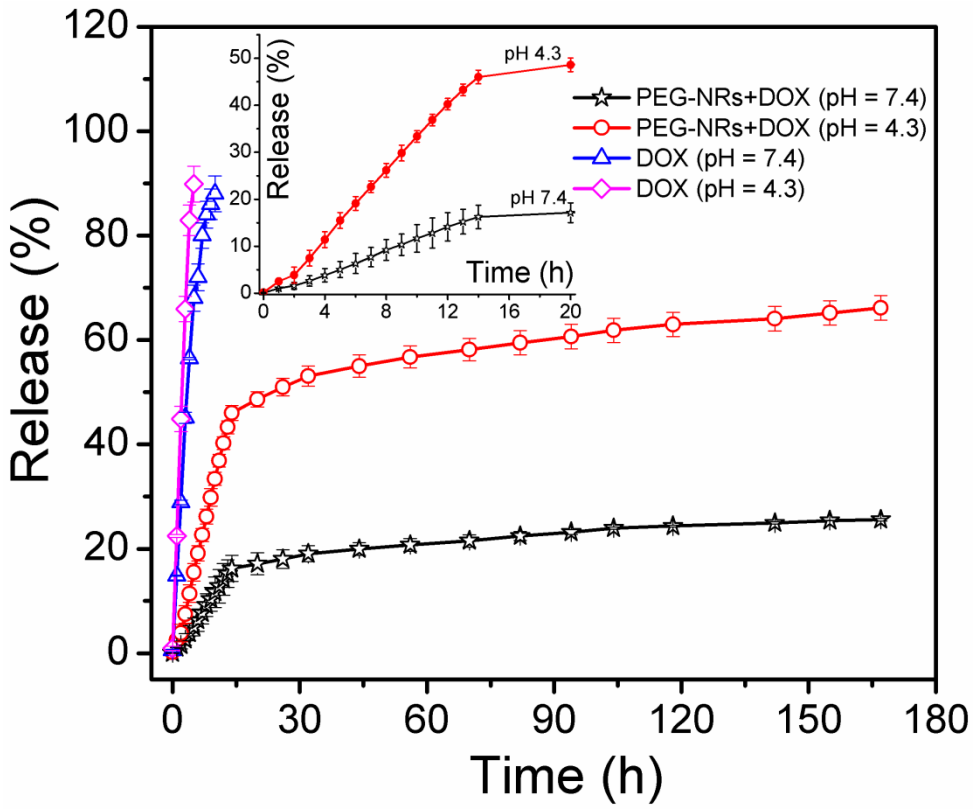

Fig. 7 Cumulative drug release profile from PEG-NRs+DOX and bare DOX at pH 7.4 and 4.3 in cell mimicking environment with PBS solution taken as reservoir. Inset: expanded view of the DOX release at pH 7.4 and 4.3 in 20 hour's duration.

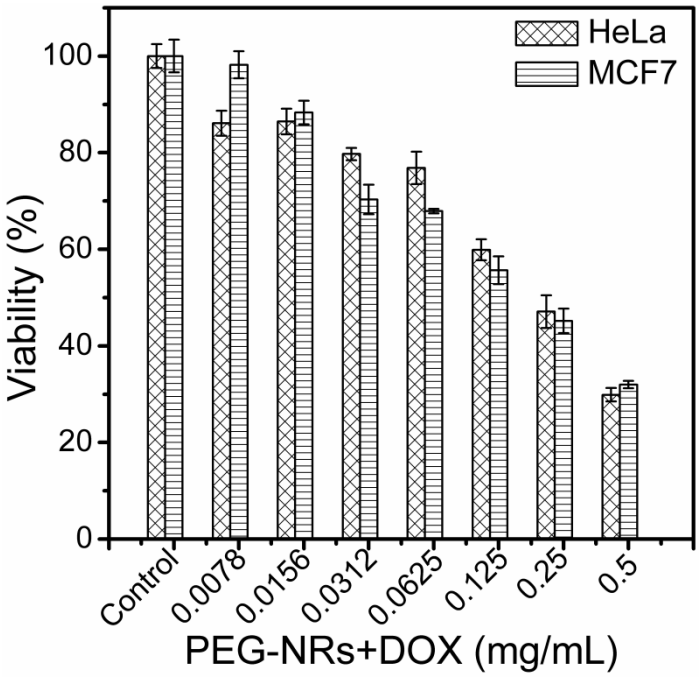

Fig. 8 *In vitro* cytotoxicity of HeLa and MCF-7 cells after incubating with different concentrations of PEG-NRs+DOX. Incubation period was 24 h in all cases.

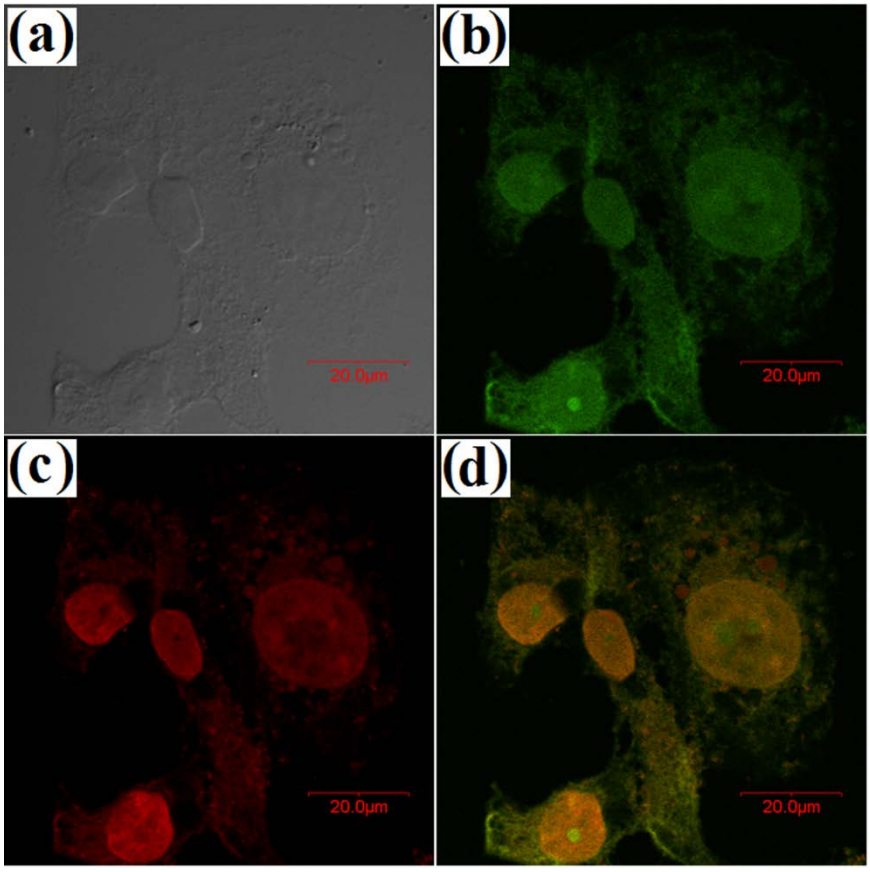

Fig. 9 CLSM images of HeLa cells showing the cellular uptake of PEG-NRs+DOX after incubation for 4h: (a) bright field image, (b) fluorescence from PEG-NRs (green), (c) fluorescence from DOX (red), (d) merged image of all the three fluorescence fields (a, b and c). All scale bars are 20 μm.

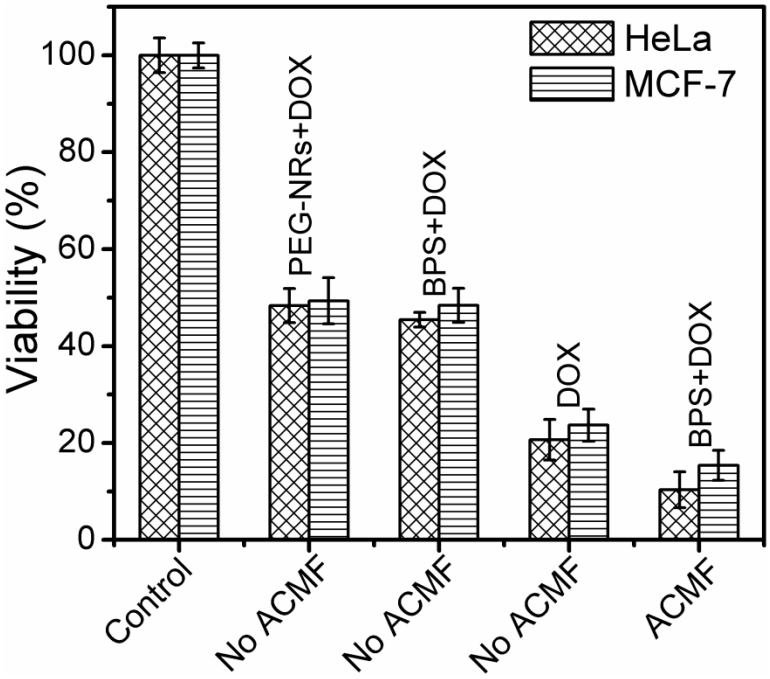

Fig. 10 *In vitro* cytotoxicity to HeLa and MCF-7 cell lines with PEG-NRs+DOX, BPS+DOX (No ACMF), bare DOX (1.2 μg) and BPS+DOX (with ACMF) during 24 h.

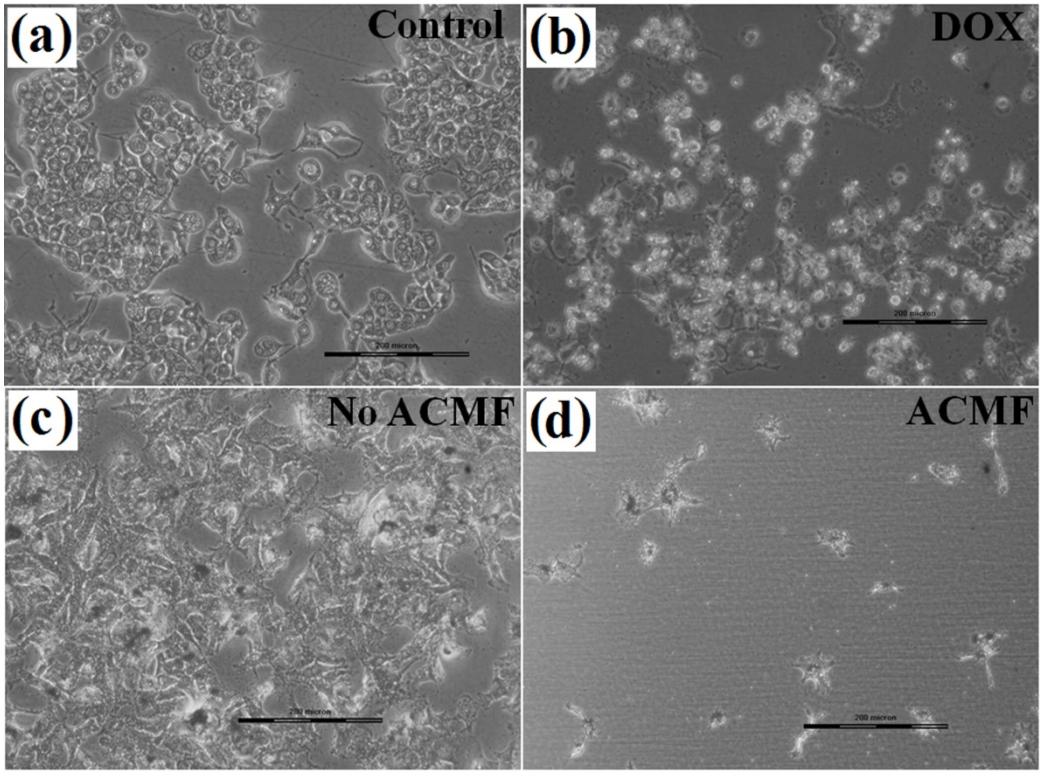

Fig. 11 Microscopic images of HeLa cells: (a) control, (b) after treatment with bare DOX, (c) after treatment with BPS+DOX and (d) after treatment with BPS+DOX in presence of ACMF. All scale bars are 200 μm.

Graphical Abstract

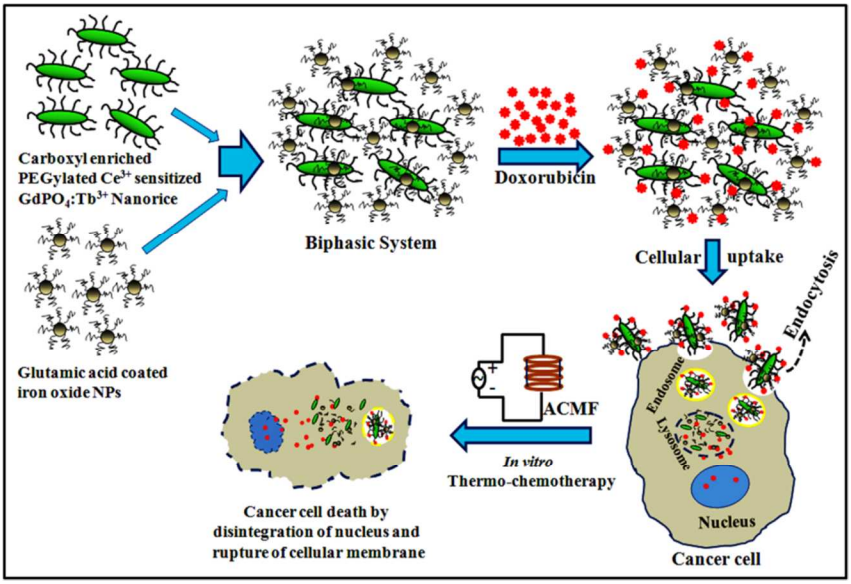

Scheme 1 Schematic representation of carboxyl enriched PEGylated Ce^{3+} sensitized $GdPO_4:Tb^{3+}$ nanorice (PEG-NRs) and its biphasic system (BPS) with glutamic acid coated iron oxide nanoparticles (IONPs) for the evaluation of their efficiency for chemo-thermal treatment against cancer cells.